Generation of Remote Homogeneous Magnetic Fields

Yuly M. Pulyer, *Life Member, IEEE,* and Mirko I. Hrovat

Abstract—This paper presents a magnetic efficiency model for comparing efficiencies of various magnets for magnetic resonance imaging. It demonstrates that monohedral magnets, magnets with sources on one side, can generate remote saddle points in the field profile relatively efficiently. These magnets may be modeled by a minimum of two magnetic dipoles. The paper examines the field profile and magnetic dipole efficiency for the two-dipole model in detail, and develops some fundamental properties of homogeneous magnetic fields.

Index Terms—Field homogeneity, magnetic resonance imaging, magnets, MRI, remote fields.

I. INTRODUCTION

FOR MANY applications, it has become increasingly important to consider magnet designs which provide convenient access to the target region of the magnet, usually the center of the magnet structure [1]–[3]. The target region may be defined as the volumetric region which has the desired magnetic field profile for an application. In the case of MRI magnets, it is desirable for the target region to be homogeneous within some specification. Magnet designs have generally consisted of either two-sided (two poles) or cylindrical structures. The suffix "hedral," from the Greek "hedron" meaning "side" or "seat," is used to describe in a simplistic manner the different types of magnets which may be designed. The traditional electromagnet with its two pole faces may be described as a "bihedral" magnet while the cylindrical solenoid may be viewed as an infinite sided "polyhedral" magnet. Currently, in order to provide convenient access to the target region, various bihedral magnets have been used [1]–[7]. Recently, another type of magnet has been proposed which provides even more "open" access. This is achieved by placing the magnetic sources to one side; hence, they are "monohedral" [8]–[15]. These "monohedral" magnets have also been termed "unilateral" [8] and "planar" magnets [12]–[15]. A monohedral magnet has a target region which is not within the magnet structure. Thus, the target region may be considered to be external or "remote" from the magnetic sources. The term "remote" is used to indicate that the target field is not encircled or enclosed by the magnetic field sources, whether they consist of currents or magnetic dipoles. Thus, a "remote" target region is more accessible or "open." It may seem unlikely that a monohedral magnet can produce a remote homogeneous field and it may be expected that the magnet is less energy efficient. However, accessibility to the target region lessens the importance for energy efficiency, and hence, the investigation of these types of magnets is worthwhile. Furthermore, as will be shown, the loss in efficiency for an open magnet may be small.

II. OVERVIEW OF MAGNET TYPES

A. Magnet Configurations

To lay the groundwork for the design of "open" magnets, we present an overview of several magnet configurations. This overview has been essential in recognizing key aspects in magnet design and has provided a method for classification of different magnet types. Several magnet structures are presented in Fig. 1, superimposed with their corresponding magnetic field profiles. Within each figure an equivalent dipole representation and an *extrema map*, which is discussed below, are provided.

Consider the traditional single solenoid magnet as shown in Fig. 1(A) [16]. It produces an internal axial field which has a maximum along the axis at the center of the coil. If the axial field profile is considered in a radial direction, then the axial field is a minimum at the center of the coil. This center point is more accurately described as a saddle point with the concomitant property that the first spatial derivatives are zero. The prior literature defines the order of a magnet in terms of the order of the derivative which is first not equal to zero at the center of the homogeneous region [17], [18]. Hence, a region homogeneous to third order has the first and second derivatives of the field profile at the center equal to zero. By this convention a first order magnet has no derivative components equal to zero. Preferably, the order of a homogeneous region may be defined in terms of the number of successive derivatives that are equal to zero at the center of such a region. In this paper, we adopt this convention, whereby the number of successive derivatives equal to zero will specify the "derivative order" of the magnet. Hence, the example of the third order magnet may be specified as having a second derivative order region. Furthermore, in regard to the solenoid of Fig. 1(A), it is noted that the external field profile of the solenoid has no saddle points and decays asymptotically to zero from the external surface of the coil.

A representation of these features is presented in Fig. 1(A) as an *extrema map*. The map is a schematic representation of the relative locations of maxima, minima, and saddle points in the magnetic field profile. Qualitatively the map also serves as a "fingerprint" for the magnetic field profile and thus for a magnet configuration. Saddle points are indicated with an "X" symbol while points of field maxima and minima (minimax points) are indicated with a solid circle, "●". Maxima and minima are located at the inner and outer surface of the solenoid. Both of these extrema are simultaneously indicated with a single solid circle. The location of a maximum or minimum near a magnetic source is a consequence of the divergence of the field being equal to zero in free space. Thus, maxima and minima only exist adjacently to sources. Since the solenoid has cylindrical symmetry,
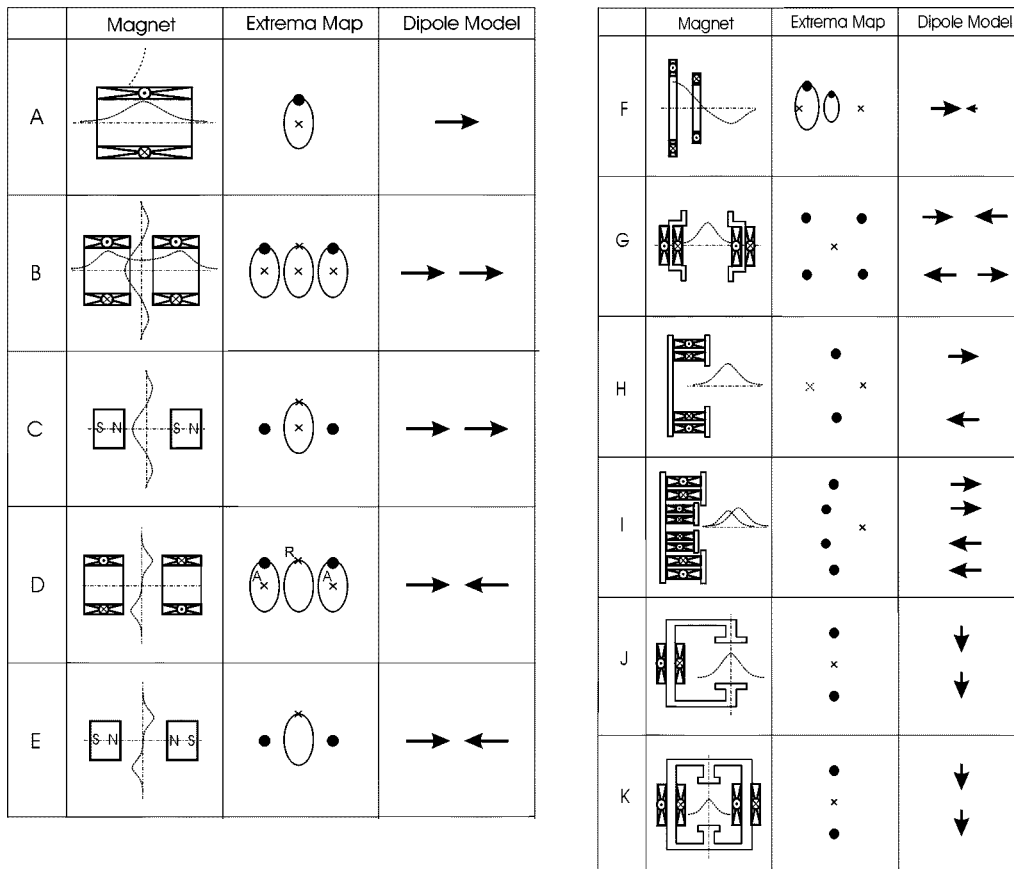
Fig. 1. Illustration of several magnet designs with qualitative field profiles. An extrema map and equivalent dipole schematic of each magnet is provided. (A) Solenoid. (B). Split-coil. (C) Split permanent magnet. (D) Opposed coil. (E) Opposed permanent magnets. (F) Pan-cake coil. (G) Bihedral iron core magnet. (H) Monohedral iron core magnet. (I) Four-dipole monohedral magnet. (J) C-magnet. (K) Double C-magnet.

these points actually form a ring. The cylindrical symmetry is schematically indicated with the ellipse while the filled circle on the ellipse indicates that the ring is a ring of maxima and minima, (a minimax ring). The use of the ellipse to represent circular or elliptical symmetry may be extended to represent a ring of saddle points or even a ring of dipoles. The choice of view-plane for the extrema map may be simply determined as the orientation which produces the greatest number of features.

In addition, the external field profile is analogous to that created by a single magnetic dipole and hence the solenoid may be equivalently represented as a single dipole, as shown in Fig. 1(A). It is necessary to point out that the extrema map of the solenoid is not accurately given by a single dipole. As the diameter of the solenoid decreases, the minimax ring and saddle point collapse to a single minimax point. Thus, in terms of the remote field behavior a minimax ring encircling a saddle point is equivalent to a magnetic dipole, as represented by a single minimax point.

If the solenoid is split into two parts as illustrated in Fig. 1(B), then the external field profile radically changes. The external field has a saddle ring (a ring of saddle points) which encircles the center of the coil pair while along the axis there are three saddle points, which exist at the extrema of the axial field profile. Since this split-coil design provides physical access to the central saddle point region, it is in use currently for magnetic resonance therapy (MRT) applications [1]–[3]. The dipole

equivalent of the split-coil consists of two colinear dipoles as is shown in Fig. 1(B). A permanent magnet analog of the split-coil magnet is shown in Fig. 1(C) and has been proposed for a miniature endoscopical MRI magnet design for external imaging [19]. The dipole equivalent of this magnet is the same as that of the split-coil magnet, though the external saddle ring is being used in this application instead of the central saddle point. Thus both of these magnets, split-coil and split-magnet, may be classified as a colinear dipoles magnet type.

From these examples, a simple rule may be generated which allows us to create the equivalent dipole model from the extrema map. A dipole may be substituted for every solid circle and for every minimax ring. It is not necessary that the minimax ring encircles a saddle point. The orientation of the dipoles is then determined by the location of the saddle points.

If the current polarity is reversed in one of the coils to create an opposed-coil magnet [Fig. 1(D)], then an external saddle ring is created for the radial field component [20]. This is clearly shown in the extrema map. The orientation of the field at the saddle point may be evident, but for added clarity it may be desirable to label the two saddle points, as we have in Fig. 1(D), with an "A" to indicate that the field is aligned along the axial direction while the saddle ring is labeled with an "R" for a field aligned along a radial direction. A permanent magnet analog also exists [Fig. 1(E)] for a medical application [7] and is in use for an industrial application (21). These two magnets may be

classified as a colinear opposed dipoles magnet type as given by their dipole model. A further generalization of the opposed-coil design leads to the magnet depicted in Fig. 1(F). The difference in diameters (or ampere-turns) of the two coils provides a shift of the saddle point with one of the saddle points moving to a point external to the two coils [8]. The concept has been further expanded as "Pan Cake" superconductive magnets [9], [11]. Again, the dipole equivalent is represented by two colinear opposed dipoles; however, one is now larger than the other. For completeness, it should be mentioned that there is a magnet design based upon two unequal colinear dipoles [10]. This design is unusual in that a saddle point is not directly generated. Instead the field has a static linear gradient which can be cancelled dynamically by gradient coils.

All of the magnets mentioned above have dipole equivalents which are represented by colinear dipoles. The bihedral geometries of Fig. 1(B) and (C) produce a field which is parallel with the symmetry axis of the magnet. Fig. 1(G) illustrates a bihedral geometry that produces a field which is parallel with the sides of the magnet [6]. In this case the bihedral magnet has a ferromagnetic core. A saddle point is found centrally between the two pole pieces. Like the split-coil design [Fig. 1(B) and (C)] the magnet does provide some limited access to the central region. The equivalent dipole model is more complex since four dipoles are now needed to represent the configuration. If half of the magnet is removed, say for example the right half, then there will remain a saddle point at the same position. This feature is preserved in the equivalent dipole representation since removal of two of the dipoles in the right half still preserves the saddle point. This is not true for any of the prior magnets considered. The monohedral design created by removal of half of the magnet is shown in Fig. 1(H) [13]–[15]. In this case, the dipole equivalent is analogous to that in Fig. 1(D) and (E) with rotation of the dipoles by 90° (antiparallel dipoles). Without an iron return, another saddle point would be present, as is shown by the dashed "X" in the figure. This is the expected map that would be obtained by two antiparallel dipoles. With the presence of the iron return, only one saddle point exists.

A better understanding of how a remote field is generated by the magnet in Fig. 1(H) is provided by Fig. 2. In Fig. 2 a superimposed pair of rectangular current loops is depicted. In this orientation, the net magnetic field is zero. As one shifts the two coils with respect to each other, two remote saddles point are generated. Eventually, as the separation increases, a maximum value is reached which then diminishes as the separation is increased further. The contribution of each current element to the total field is depicted in Fig. 3. Even though this type of configuration for a magnet is expected to be more efficient than the opposed coil or "Pan Cake" magnet [Fig. 1(F)], there can be perceived an inefficiency due to the pairing of the current wires in the pole faces. In Fig. 3, the contributions of the four current wires to the net magnetic field are shown vectorially. The two current wires in the center contribute to B_{z1} while the two outer current wires contribute to B_{z2}. Clearly the magnet efficiency can be increased by reducing B_{z2}. This could be achieved by moving the outer current wires farther out, but at the expense of increasing perimeter copper losses.

As Fig. 2 is instructive in understanding the field produced in Fig. 1(H), Fig. 4 is instructive in understanding the field pro-
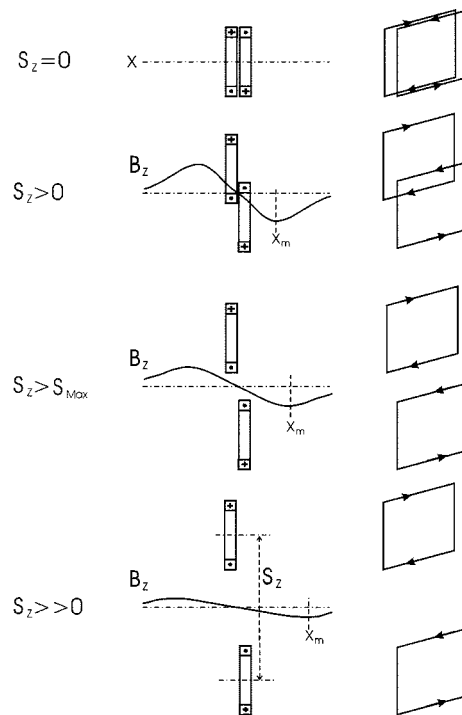

Fig. 2. Illustration of how two coils shifted in the plane of the coils produces a remote saddle point.
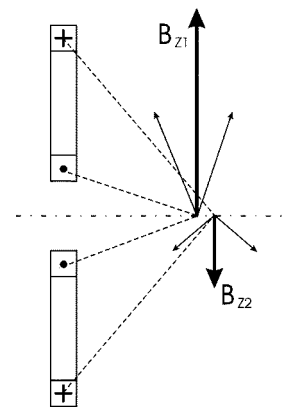

Fig. 3. Contribution of the horizontal current elements to the magnetic field for the two coils of Fig. 2.

duced by the coil pair in Fig. 1(B). In Fig. 4, a superimposed pair of rectangular current loops are oriented horizontally. Unlike Fig. 2, the top configuration of Fig. 4 produces a net magnetic field without a remote saddle point. As one shifts the two coils axially with respect to each other, two remote saddle points are generated. Eventually, as the separation increases a maximum value is reached which then diminishes as the separation is increased further. As in Fig. 2, the field maximum is a function of two parameters, the separation (S_z) and one dimension, a, of the coils. The contribution of each current element to the total field is depicted in Fig. 5. Again there can be perceived an inefficiency due to the pairing of the current wires. The two current wires on the right contribute to B_{z1} while the two current wires on the left contribute to B_{z2}. The magnet efficiency could be increased by reducing B_{z2}, analogously as above.
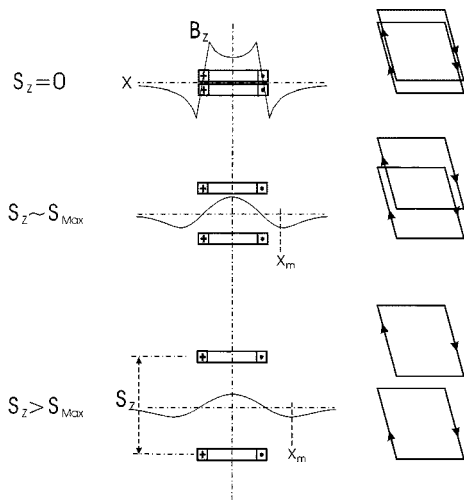
Fig. 4.   Illustration of how two coils shifted perpendicular to the plane of the coils produces a remote saddle point.
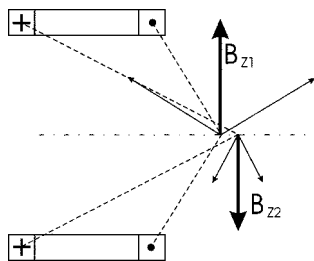

Fig. 5.   Contribution of the horizontal current elements to the magnetic field for the two coils of Fig. 4.

A further improvement to the monohedral magnet of Fig. 1(H) is shown with the planar magnet depicted in Fig. 1(I) [15]. Here, the magnet consists of a pair of opposed magnetic dipole sources located between another pair of opposed magnetic dipole sources. This is clearly seen in the dipole model for the magnet. The additional inner magnetic sources may be considered as a second magnet whose saddle point is at a different location from that created by the outer magnetic sources. The total magnetic field then has a larger region of homogeneity with the saddle point for the total field differing from the location of the saddle point of the individual magnets. Clearly this design illustrates conceptually that monohedral magnets are shimmable through additional magnetic sources. A further advantage to this type of magnet is that the leakage between the pole pieces is reduced as the reluctance of the gap between the inner and outer magnet is increased. Contrast this with the magnet of Fig. 1(H) which has undesirable flux leakage losses along its edges.

For completeness, consider the magnets depicted in Fig. 1(J) and (K). The magnet in Fig. 1(J) is a traditional C-magnet while the magnet in Fig. 1(K) has the added advantage of symmetry and better homogeneity. The former magnet has found application as an open magnet for MRI/MRT applications [3] while an extension of the latter design to fourfold symmetry is also available commercially [3]. Both magnets may be simply represented with two colinear dipoles. Thus, these magnets may be classified with those of Fig. 1(A) and (B). Note that rotating the

pole faces of the C-magnet by $90°$ converts the magnet to the type represented by Fig. 1(H).

The extrema maps and the dipole models help classify the various magnet geometries. For example, based upon dipole models, magnets may be classified as colinear dipoles, opposed colinear dipoles, antiparallel dipoles, and combinations of them. For most cases, the extrema maps permit a similar interpretation. Colinear dipoles produce maps whereby the saddle point is colinear with the minimax points. On the other hand, two of the opposed colinear dipoles [Fig. 1(D) and (F)] produce strikingly different extrema maps. The monohedral type is more perceptible from the extrema map perspective. If a saddle point exists such that it is not colinear with the minimax points, then the magnetic sources will be located to one side. That configuration may then be considered as a monohedral type as seen in Fig. 1(F), (H), and (I). Based upon the magnets introduced above, it is clear that a suitable monohedral magnet will have the following features. 1) It must generate a remote saddle point. 2) The dipole analog of the monohedral magnet will likely consist of antiparallel dipoles or opposed colinear dipoles. 3) Current elements and/or magnetic materials may be employed to achieve similar classes of magnets independent of the technology employed.

B. Magnet Efficiency

It is not appropriate to discuss various magnet configurations without considering relative magnetic efficiency. This type of comparison is difficult because it is not apparent which magnetic parameters should be utilized toward a measure of efficiency. For example, a particular magnet configuration may be suitable in terms of the size of target region provided, field strength, and "openness" (accessibility to the target region), and yet may not be suitable if it requires a large input current. Likewise, a magnet which may utilize less current for the same field strength may provide a smaller target region. Another magnet may be a permanent magnet design while another uses superconducting coils. Nevertheless, the ratio of field strength in the target region (B_0) to some measure of the driving magnetomotive force provides a fundamental, though simple, measure of magnet efficiency. Thus, we consider magnet efficiency as the ratio of B_0, the mean value of the magnetic field in the target region, to $\mu_o IN$ or $\mu_o mN$. IN represents the total ampere-turns for the case of current sources and mN represents the total magnetic moment for the case of dipole sources. Thus

$$IN \equiv \sum_k I_k \quad mN \equiv \sum_k m_k \tag{1}$$

and the total magnetomotive force is given by summing over all of the individual current and dipole sources. Since the magnetic moment of a current loop is given by $m_k = I_k A_k$ where A_k is the area of the loop, then we have the additional relationships

$$mN = \sum_k I_k A_k \equiv A \times IN$$

$$A = \sum_k \frac{I_k}{IN} A_k \tag{2}$$

where A is defined as the total effective area. The value of B_0 may be given by

$$B_o = \mu_o I N f_I(r_{tp}) = \mu_o m N f_D(r_{tp}) \qquad (3)$$

where $f_I(r_{tp})$ and $f_D(r_{tp})$ represent the field transfer function at the target point for current and dipole sources, respectively. Thus, the current and dipole magnetic efficiency are defined by

$$e_I = \frac{B_o}{\mu_o I N} = f_I(r_{tp})$$

$$e_D = \frac{B_o}{\mu_o m N} = f_D(r_{tp}) \qquad (4)$$

with $e_I = A e_D$.

With the developed framework for efficiency, it is possible to compare the relative efficiencies of the different magnet configurations. Table I presents at quick glance at current and dipole magnetic efficiencies for various magnet configurations. For some configurations, a direct comparison between current and dipole magnetic efficiency is difficult, as the comparison requires a value for the equivalent radius of the current loop of a dipole. However, it is possible in all cases to compare the dipole magnetic efficiency between different configurations. The solenoidal case illustrates that the efficiency is inversely correlated with the length of the solenoid. Colinear dipoles which use the central saddle point are also quite efficient in contrast to the saddle ring which has poor efficiency. At first glance the Helmholtz pair seems to have good efficiency when compared with colinear dipoles; however, the separation between the coils is equal to a whereas the separation between the dipoles is equal to $2a$. A current loop of radius R is similar to a dipole in field strength only for the far field, $(a > R)$. In the near field the current loop is weaker by the ratio $a^3/(R^2 + a^2)^{3/2}$. Antiparallel dipoles and opposed dipoles have identical efficiencies, while unequal opposed dipoles are clearly inefficient. The case for unequal opposed dipoles is a simplification for the magnet configuration of unequal opposed coils [see Fig. 1(F)] as analytic forms for saddle point position and field intensity do not exist for the latter [8].

It may be argued that the degree of openness is not identical among the various magnet configurations. One method to equalize openness would be to define the distance from the saddle point to the nearest magnetic source to be equal to some fixed value, "a." This method has the merit of insuring that magnetic sources are excluded from a minimal sized sample region. It may still be argued that even under these conditions some magnet configurations are still more open than others. Nevertheless, the above definition provides a quantitative reference frame to evaluate efficiency. The last column in Table I provides the recalculated relative dipole efficiencies for equal openness. The efficiency of the colinear dipoles remains the same if the central saddle point is used. The greatest improvement occurs for the saddle ring of the colinear dipole where the spacing is reduced from $2a$ to $0.89a$. The Helmholtz coil pair improves due to a reduction in size of the coil by 10.6%. With the stipulation of equal openness, the apparent disparity in efficiency between the dipole and current loop disappears. The antiparallel and op-

posed dipoles increase in efficiency while the unequal opposed dipoles still remain inefficient.

From an inspection of the table, several general observations may be made. 1) "Open" magnet configurations are not grossly inefficient as compared with more "closed" configurations. 2) Dipole sources are potentially more efficient. Since dipole sources imply permanent magnets and electromagnets while current sources imply resistive and superconducting magnets, then this statement is tempered by the fact that material properties may limit the magnetic moment strength for permanent magnets and electromagnets, while superconducting magnets have a wide range of current strengths. 3) Differential configurations such as the unequal opposed dipoles are clearly inefficient. 4) The saddle point, if it exists, generated in the magnetic return path is less efficient then a saddle point that exists in the closer primary magnetic flux path.

III. MAGNETIC FIELD BASICS

A. Description of the Magnetic Field

A homogeneous field may be defined as a field that is fairly constant in magnitude and nearly unidirectional in some region of space. As was mentioned above, it is desirable that the homogeneous field be of high order. This corresponds to having several higher order derivatives of the field at the origin of the target field to be equal to zero. The higher order terms may be set to zero by either careful magnet design or through a process referred to as "shimming." Shimming may be applied with additional coil sets, (such as resistive and/or superconducting coils), and/or magnetic materials, (such as steel or permanent magnets) [18], [23]. Since the shimming process is a perturbation to the overall field, it is important that the main magnetic field be sufficiently homogeneous. Otherwise, the amount of energy allocated to shimming will not be small compared to the main magnetic field, and the shim coils should then be considered an integral part of the magnet design. In the sense of a perturbation, shimming cannot compensate for a flawed magnet design. Therefore, a minimal requirement for a magnet design is that it must generate at least a first derivative order saddle point. A high order magnet design will not only contain a saddle point, but will also have a larger target region relative to the size of the magnet.

For any magnetic field in free space, Maxwell's equations must be obeyed. In turn, these equations allow the determination of several important properties for magnetic fields regardless of how they are generated. In free space the magnetic field may be described with a scalar potential, $\Phi(\vec{r})$, to give $\vec{B}(\vec{r}) = \vec{\nabla}\Phi(\vec{r})$ and along with Maxwell's equations we have
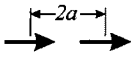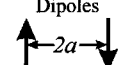
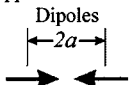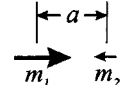$$\nabla^2 \Phi(\vec{r}) = 0 \qquad (5)$$

where the magnetic scalar potential satisfies Laplace's equation. Consequently, each component of the magnetic field also must satisfy Laplace's equation as summarily given by

$$\nabla^2 \vec{B}(\vec{r}) = 0. \qquad (6)$$

Unfortunately the magnitude of the field does not satisfy Laplace's equation, i.e., $\nabla^2 B(\vec{r}) \neq 0$, and knowledge of the

TABLE I

MAGNETIC EFFICIENCY OF VARIOUS MAGNET CONFIGURATIONS. DISTANCE TO SADDLE POINT IS FROM THE GEOMETRIC CENTER OF THE MAGNET CONFIGURATION. "EQUAL OPENESS" IS DEFINED AS SETTING THE DISTANCE FROM THE SADDLE POINT TO THE CLOSEST MAGNETIC SOURCE TO EQUAL a. NOTE: $\pi R^2 = mN/IN$

Magnet Configuration	Distance to Saddle	e_I	e_D	relative e_D	rel. e_D equal openness
Solenoid $(R=a)$	0	$\dfrac{1}{2a}\dfrac{1}{\sqrt{1+(L/2a)^2}}$	$\dfrac{1}{2\pi a^3}\dfrac{1}{\sqrt{1+(L/2a)^2}}$	70.7%‡	70.7%‡
Co-linear Dipoles	0	$\dfrac{R^2}{2a^3}$	$\dfrac{1}{2\pi a^3}$	100.0%	100.0%
($\leftarrow 2a \rightarrow$)	$2a^*$	$\dfrac{R^2}{2\,5^{5/2}a^3}$	$\dfrac{1}{2\pi\,5^{5/2}a^3}$	1.8%	20.0%
Helmholtz Pair $(R=a)$	0	$\dfrac{4}{5^{3/2}a}$	$\dfrac{4}{\pi\,5^{3/2}a^3}$	71.6%	100.0%
Anti-parallel Dipoles ($\leftarrow 2a \rightarrow$)	$\dfrac{a}{2}$	$\dfrac{12R^2}{5^{5/2}a^3}$	$\dfrac{12}{\pi\,5^{5/2}a^3}$	42.9%	60.0%
Opposed Co-linear Dipoles ($\leftarrow 2a \rightarrow$)	$\dfrac{a}{2}$ •	$\dfrac{12R^2}{5^{5/2}a^3}$	$\dfrac{12}{\pi\,5^{5/2}a^3}$	42.9%	60.0%
Unequal Opposed Co-linear Dipoles ($\leftarrow a \rightarrow$) $m_1\quad m_2$	$\dfrac{a}{1-(m_2/m_1)^{1/4}}$ **	$\dfrac{R^2}{2a^3}\dfrac{(m_1^{1/4}-m_2^{1/4})^4}{m_1+m_2}$	$\dfrac{1}{2\pi a^3}\dfrac{(m_1^{1/4}-m_2^{1/4})^4}{m_1+m_2}$	3.3%†	7.0%††

 * This is the radius of the saddle ring.

 ** Saddle distance is relative to the center of m_1.

 ‡ Calculated for $L = 2a$.

 † Calculated with: $m_1/m_2 = 10$; *Saddle distance from $m_1 = 2.28a$.*

 †† Calculated with: $m_1/m_2 = 10$; *Saddle distance from $m_1 = 1.78a$.*

magnitude of the field is desirable for MRI applications. It is convenient that any component of the field may be expanded in terms of any basis set (spatial harmonics) which also satisfies Laplace's equation. For example, it is common to perform an expansion in terms of spherical harmonics such as

$$B_z(r,\theta,\varphi) = B_0 \sum_{l=0}^{\infty} \sum_{m=0}^{l} \left(\frac{r}{r_0}\right)^l \frac{P_{lm}(\cos\theta)}{N_{lm}} \times [A_{lm}\cos(m\varphi) + B_{lm}\sin(m\varphi)] \quad (7)$$

where the coefficients in the expansion are given by A_{lm} and B_{lm} [18], [23], [24]. This basis set is known as the Legendre functions of the first kind, but are more commonly referred to as tesseral harmonics for $m < l$ and sectoral harmonics for $m = l$. The case $m = 0$ is also referred to as zonal harmonics. B_0 is the value of the field at the center and the P_{lm} are the associated Legendre polynomials with N_{lm} representing a convenient normalization factor. The expansion is normalized with respect to a sphere of radius, r_o, which defines the target region size. The expansion rapidly converges with respect to l for $r < r_o$. The particular form shown in (7) has the advantage that the co-

efficients can have the dimensions of parts per million (ppm). If N_{lm} is chosen to be

$$N_{lm} \equiv \sqrt{\frac{4\pi(l-m)!}{\epsilon_m(2l+1)(l+m)!}} \quad (8)$$

where ϵ_m is Neumann's factor ($\epsilon_m = 2$ for $m \neq 0$ and $\epsilon_m = 1$ for $m = 0$), then the statistical error estimate of the harmonic coefficients will be constant with increasing l and m. When the iterative process of shimming has produced harmonic coefficients that fall within the error estimates, then further reduction is not realistically possible [24].

B. Saddle Points

If the field is homogeneous within a region of space, it is expected that $\vec{\nabla} B_i = 0$ at some central point within the region. Equation (6) suggests that any component of the field also satisfies a curvature relation of the form

$$\frac{d^2 B_i}{dz^2} = -\left[\frac{d^2 B_i}{dx^2} + \frac{d^2 B_i}{dy^2}\right]. \quad (9)$$

Therefore, if a component of the field exhibits a positive or negative curvature along z then there must be an equal and oppo-

site curvature of that component of the field perpendicular to z. There is no absolute maximum or minimum in the field though there may be a maximum or minimum with respect to a particular coordinate. If $\vec{\nabla} B_i = 0$ at a particular point in space then it must be a saddle point. This in turn implies that any homogeneous region must begin about a saddle point. Since each component of the field satisfies Laplace's equation, then the derivatives of the field component must also satisfy Laplace's equation. In Appendix A, it is shown that there is an equivalence to the nth spatial derivative at the origin of the target region to the nth order terms in the spherical harmonic expansion. The convention used for an Nth derivative order magnet corresponds to a configuration whereby all terms in the spherical harmonic expansion are zero for all m for $l = 1$ to N.

C. Unidirectionality of Homogeneous Fields

Consider a very small region of space where the magnetic field is unidirectional but may not necessarily be constant in magnitude. Let the z axis be defined to be parallel to the direction of the magnetic field so that $B_x = B_y = 0$. Then, by Maxwell's equations

$$-\frac{\partial B_z}{\partial z} = \frac{\partial B_x}{\partial x} + \frac{\partial B_y}{\partial y} \quad \frac{\partial B_z}{\partial x} = \frac{\partial B_x}{\partial z} \quad \frac{\partial B_z}{\partial y} = \frac{\partial B_y}{\partial z}. \quad (10)$$

Because the field is unidirectional along z, then $\vec{\nabla} B_x = \vec{\nabla} B_y = 0$ and from the above equation, $\vec{\nabla} B_z = 0$. Therefore, B_z must be constant. *Thus, a unidirectional field must be constant in magnitude.*

Now consider a very small region of space where the magnetic field is constant in magnitude, B, but may not necessarily be unidirectional. Furthermore, if s_i is a measure of length along the ith coordinate direction, then the relation

$$\frac{\partial B}{\partial s_i} = \frac{\vec{B}}{B} \cdot \frac{\partial \vec{B}}{\partial s_i} = 0 \quad (11)$$

implies that a homogeneous field may only have spatial varying components that are orthogonal to the direction of the field. Since the curl of the field is zero, it can be shown that

$$\frac{\partial \vec{B}}{\partial s_i} = \vec{\nabla} B_i. \quad (12)$$

However, by (11), the change of any field component along the direction of the field must be zero. For example, if we define the field to be aligned along the z axis at a particular point in space, then $\vec{\nabla} B_z = 0$. Since there is no change in the field along its direction and the magnitude is constant, then all changes in components perpendicular to the field must also be zero, i.e., $\partial \vec{B}/\partial s_i = 0$ for any direction. *Hence, a magnetic field constant in magnitude is unidirectional.* Consequently, the definition of a homogeneous field is consistent with a field constant in magnitude which then must be unidirectional.

D. Influence of B_x and B_y on Homogeneous Fields

Since there are three independent spatial components to the magnetic field, it is necessary to ask whether all three components of the field must be specified in the design of a homogeneous region. Certainly, symmetry of the source elements plays
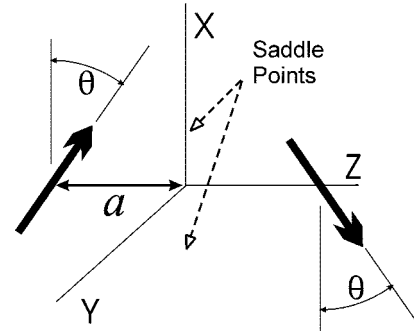

Fig. 6. Schematic representation of the two-dipole model. The two saddle points at $x = \pm a/2$ in B_z are indicated for the case $\theta = 0°$.

a role in traditional magnet design to ensure that the magnetic field is dominated by a single component. Likewise, it is expected that in the design of monohedral magnets, symmetry will play a corresponding role. For example, if the source elements are extended along the y direction, then $B_y = 0$ and $\vec{\nabla} B_y = 0$ and, only B_z needs to be considered in the design of such a magnet. An example of this is given by replacing the two dipoles in Fig. 1(H) by a string of dipoles along the y direction. There will be no variation along the y direction and B_x will only depend upon z.

It would be desirable to be only concerned with just one component of the field even in the absence of symmetry. The previous section seems to imply that it may not be necessary to specify all three components, since we may consider a constant magnetic field to be unidirectional. Therefore, if a magnetic field is nearly homogeneous, then it will be dominated by a single component, such as B_z, which is parallel to the general direction of the field. Under these conditions, the magnitude of the field, B, is given by

$$B = B_z \left(1 + \frac{1}{2} \frac{B_\perp^2}{B_z^2} + \dots \right) \quad (13)$$

where $B_\perp$ is the magnitude of the perpendicular component to the field. In order to achieve a homogeneity to a ppm, it is only necessary to reduce the perpendicular component to a part in a thousand. For these reasons, it is possible to design monohedral magnets with the same simple considerations used for traditional magnets.

IV. TWO-DIPOLE MODEL

A. Two Antiparallel Dipoles

From the prior discussion on magnet configurations, it is evident that an investigation of the two dipole configuration is worthwhile. The magnetic field of a magnetic dipole, $\vec{m}$, is given by

$$\vec{B}(\vec{r}) = \frac{\mu_o}{4\pi} \left(\frac{3\vec{r}(\vec{r} \cdot \vec{m})}{r^5} - \frac{\vec{m}}{r^3} \right) \quad (14)$$

where μ_o is the magnetic permeability of free space and m is the dipole moment strength [22]. A single dipole does not exhibit any saddle points. However, as was seen in Fig. 1, two dipoles may have saddle points. Referring to Fig. 6, consider two magnetic dipoles, oriented along the x direction ($\theta = 0°$), that are
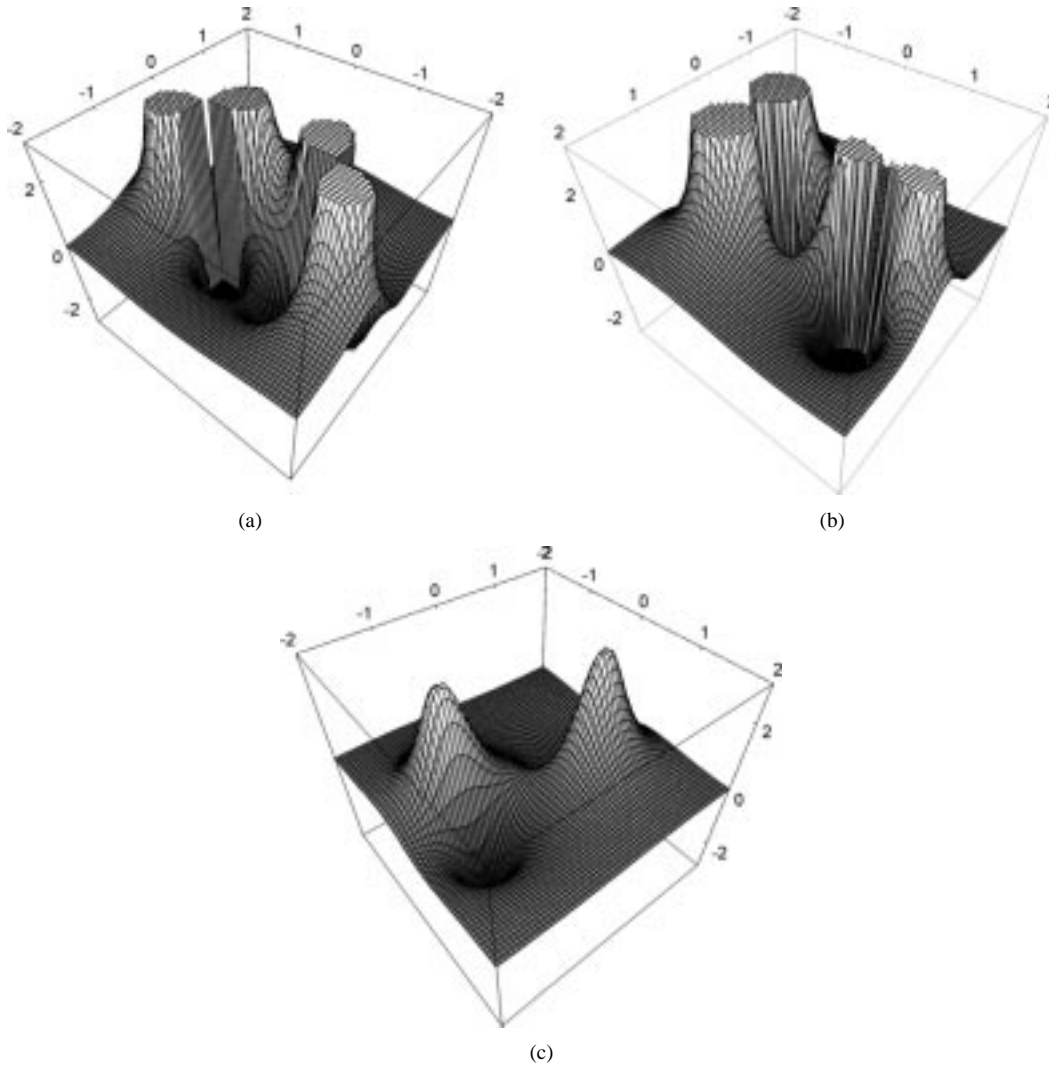
Fig. 7.   Illustration of the two-dipole field profile in the xz plane. (a) B_z component. (b) B_x component. (c) B_y component at $y = 1.6 \times 10^{-6} a$.

placed directly on the z axis at locations a and $-a$. The components of the field are then given by

$$
\begin{aligned}
B_x &= \frac{\mu_o m}{4\pi} \left[\frac{(2x^2 - y^2 - (z+a)^2)}{(x^2 + y^2 + (z+a)^2)^{5/2}} \right. \\
&\quad \left. - \frac{(2x^2 - y^2 - (z-a)^2)}{(x^2 + y^2 + (z-a)^2)^{5/2}} \right] \\
B_y &= \frac{3xy\mu_o m}{4\pi} \left[\frac{1}{(x^2 + y^2 + (z+a)^2)^{5/2}} \right. \\
&\quad \left. - \frac{1}{(x^2 + y^2 + (z-a)^2)^{5/2}} \right] \\
B_z &= \frac{3x\mu_o m}{4\pi} \left[\frac{z+a}{(x^2 + y^2 + (z+a)^2)^{5/2}} \right. \\
&\quad \left. - \frac{z-a}{(x^2 + y^2 + (z-a)^2)^{5/2}} \right].
\end{aligned}
\tag{15}
$$

The behavior of these field components is shown in Fig. 7 for $y = 0$. Since $B_y(y = 0) = 0$ for all x and z, B_y is shown for a slight offset on y. Setting the first derivatives of B_z to zero with respect to x, y, z reveals by inspection that a saddle point exists at $(\pm a/2, 0, 0)$. These points are indicated in Fig. 6 and clearly seen in Fig. 7(a). The value of B_z at these points is

$\pm 24\mu_o m/(5^{5/2}\pi a^3)$. Furthermore, B_y and B_x are both equal to zero at the saddle points so that B_z is the only contributing component. Interestingly, B_x and B_y have saddle points at $(\pm a/2, 0, 0)$ and $(0, 0, 0)$ respectively, [seen in Fig. 7(b) and (c)] but their value at these saddle points is zero. Further examination of the functional form for B_z reveals that all odd order derivatives of B_z with respect to z and y vanish at the saddle point. Therefore, two antiparallel dipoles have a first derivative order saddle point.

B. Effect of Orientation

A further refinement to the two-dipole model may be made if the orientation of the dipoles is varied. Let θ be the angle that subtends the dipoles and the x direction as shown in Fig. 6. For $\theta = \pm 90°$ the dipoles are colinear, as represented in Fig. 1(B) or (C). As above, the saddle points for B_z may be determined by setting the first derivatives to zero. The solution for saddle point position now depends on solving the following cubic equation:

$$
0 = 1 - 4\tan\theta(x/a) - 4(x/a)^2 + \tan\theta(x/a)^3. \tag{16}
$$

When $\tan\theta = 0$, a solution is given by $x = \pm a/2$ and when $\tan\theta = \pm\infty$, a solution is given by $x = \pm 2a, 0$. These two so-
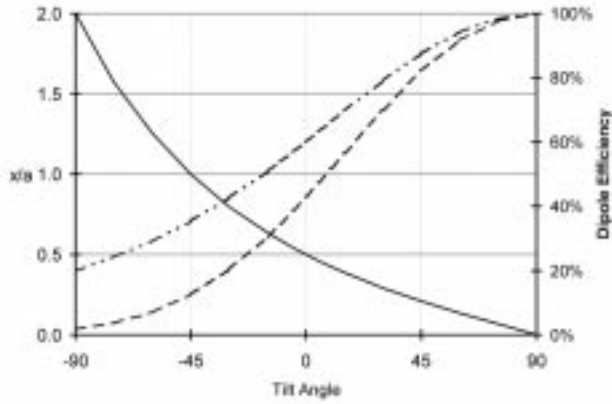
Fig. 8. Saddle point position and relative field strength (B_z) for the two dipole model as a function of tilt angle in degrees. _____ Saddle point position, _ _ _ _ _ Relative magnetic dipole efficiency, _ _ _ _ _ Relative magnetic dipole efficiency for a fixed distance between saddle point and dipoles.
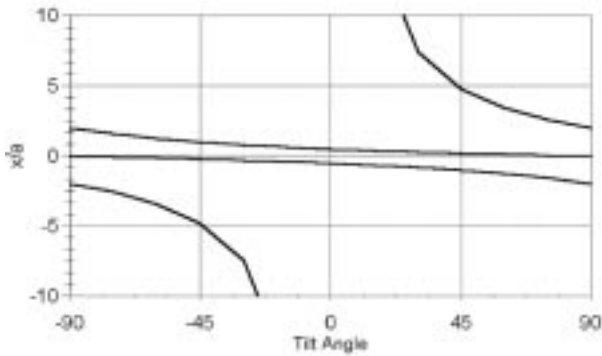

Fig. 9. Saddle point positions as a function of tilt angle in degrees for the two-dipole model. Notice that at any particular tilt angle only three saddle points exist.

lutions correspond to the orientation of the dipoles perpendicular and parallel to the z axis, respectively. The behavior of one of the roots of (16) is shown in Fig. 8, the saddle point position as well as the magnetic dipole efficiency varies with θ. As before, if the dipole efficiency is adjusted for a constant fixed distance from the dipoles to the saddle point, then the dipole efficiency will increase as the saddle point moves farther away from the yz plane (see Fig. 8). Thus, orientation provides another degree of freedom to control either saddle point location or efficiency. This simple example illustrates that there is considerable flexibility in controlling the position of the saddle point. The saddle point positions as given by the three roots of (16) are shown in Fig. 9.

V. SHIMMING THE MAGNETIC FIELD AND THE FEASIBILITY OF MONOHEDRAL GRADIENT COILS

Clearly, the theoretical feasibility of a remote homogeneous target magnetic field depends upon the existence of an external saddle point. This provides a core of homogeneity. Standard techniques for magnetic field shimming may then be used to increase the size of this core field [18], [23]. Both shimming and the application of gradients (in MRI) generate a correction to the magnetic field in order to generate a desired field pro-

file. In principle, either method can be implemented through the use of current elements and/or ferromagnetic materials. In those applications where the field profile changes dynamically, as in MRI, the use of current elements is more practical. However, the design process in either case is similar. To illustrate the feasibility of shimming an external field generated by a monohedral magnet, consider the field to be expressed in terms of spherical harmonics as in (7). In this example, ferromagnetic shimming techniques will be employed. The field generated by a distribution of magnetic dipoles is given (see [25]) by

$$B_z(r, \theta, \phi) = \frac{1}{4\pi} \sum_{l=0}^{\infty} \sum_{m=0}^{l} \epsilon_m \frac{(l-m+2)!}{(l+m)!} r^l P_{lm}(\cos\theta)$$
$$\times \mathrm{Re}\left[e^{im\phi} \int \sigma(\rho, \alpha, \beta) \frac{P_{l+2,m}(\cos\alpha)}{\rho^{l+3}} e^{-im\beta} d\rho^3 \right] \quad (17)$$

where ϵ_m is Neumann's factor, σ is the magnetic dipole density at the spherical coordinates given by (ρ, α, β), and $\mathbf{Re}[\ ]$ extracts the real part between the brackets. If our distribution of dipoles consist of only two arbitrarily located pieces of iron (reduced to infinitesimal size, ΔV), then the field contribution is given by

$$B_z(r, \theta, \phi) = \frac{1}{4\pi} \sum_{l=0}^{\infty} \sum_{m=0}^{l} \epsilon_m \frac{(l-m+2)!}{(l+m)!} r^l P_{lm}(\cos\theta)\Delta V$$
$$\times \mathrm{Re}\left[e^{im\phi} \sigma_1 \frac{P_{l+2,m}(\cos\alpha_1)}{\rho_1^{l+3}} e^{-im\beta_1} \right.$$
$$\left. + e^{im\phi} \sigma_2 \frac{P_{l+2,m}(\cos\alpha_2)}{\rho_2^{l+3}} e^{-im\beta_2} \right]. \quad (18)$$

This may be summarily rewritten as

$$B_z = \sum_{l=0}^{\infty} \sum_{m=0}^{l} r^l P_{lm}(\cos\theta) \left[C_{lm}^1 \cos(m\varphi) + D_{lm}^1 \sin(m\varphi) \right.$$
$$\left. + C_{lm}^2 \cos(m\varphi) + D_{lm}^2 \sin(m\varphi) \right] \quad (19)$$

where

$$C_{lm}^i = \frac{\epsilon_m}{4\pi} \frac{(l-m+2)!}{(l+m)!} \frac{\sigma_i \Delta V P_{l+2,m}(\cos\alpha_i) \cos(m\beta_i)}{\rho_i^{l+3}}$$
$$D_{lm}^i = \frac{\epsilon_m}{4\pi} \frac{(l-m+2)!}{(l+m)!} \frac{\sigma_i \Delta V P_{l+2,m}(\cos\alpha_i) \sin(m\beta_i)}{\rho_i^{l+3}}. \quad (20)$$

If (19) is matched up with the expansion of the magnetic field as given by (7), then

$$A_{lm} = -\frac{r_0^l N_{lm}}{B_0} \left[C_{lm}^1 + C_{lm}^2 \right]$$
$$B_{lm} = -\frac{r_0^l N_{lm}}{B_0} \left[D_{lm}^1 + D_{lm}^2 \right]. \quad (21)$$

The minus sign reflects that to produce a homogeneous field, the shim correction must produce a harmonic coefficient opposite in sign to the value of the field harmonic. If C_{lm} and D_{lm} are not zero, i.e., are not positioned on a node, then any two harmonic coefficients may be matched with the two pieces of iron. It should be noted from (20) that C_{lm} and D_{lm} are independent of each other and that only two degrees of freedom are provided by the two pieces of iron. Thus either one A_{lm} term and one B_{lm} term, or two A_{lm} terms, or two B_{lm} terms may be matched. Thus, two pieces of steel may be used to correct for

any two harmonic terms without significant regard to their location. Clearly, this technique may be continued in an arbitrary manner with n pieces of steel in order to correct n different harmonic terms. This would produce a system of n linear equations similar in form to (21) which may then be solved by standard numerical techniques. It is expected that other methods will be developed which will improve upon the method described here and this is a matter of current investigation.

It becomes clear that monohedral magnets may achieve homogeneities comparable to whole body magnets. If a design for a planar magnet achieves a saddle point, then this saddle region may be extended by traditional methods to achieve the desired homogeneity in the target region. Similar to traditional whole body magnets, it is expected that a high derivative order saddle point will generate a larger target region than a simple first derivative order saddle point.

VI. CONCLUSION

The classification diagrams, extrema maps and dipole equivalent models, demonstrate similarities among the various magnet geometries. Those magnets which provide remote saddle points are called monohedral. These magnets have special importance for open magnet design. Furthermore, monohedral magnets are not by their nature grossly inefficient. The efficiency of monohedral magnets should compare favorably with bihedral magnets. The current or dipole magnetic efficiency may be used to compare various magnet designs. A first derivative order saddle point is established as the minimum requirement for a remote homogeneous magnetic field. Two dipoles provide the minimum configuration to produce such a field. Variation of the spacing or orientation of the dipoles provides flexibility for location of the saddle point. Through a dipole model, it is also demonstrated that shims and gradient systems may also be generated for monohedral systems. The development of an analytical methodology for monohedral magnets is of primary importance for the future of open MRI technology with enormous medical significance.

APPENDIX A
EQUIVALENCE OF SPHERICAL HARMONIC ORDER WITH DERIVATIVE ORDER

Consider a solution to Laplace's equation in terms of the spherical harmonic forms [23], [25]

$$T_{lm}^{E+}(r,\theta,\varphi) \equiv r^l P_{lm}(\cos\theta)\cos(m\varphi)$$
$$T_{lm}^{O+}(r,\theta,\varphi) \equiv r^l P_{lm}(\cos\theta)\sin(m\varphi)$$

$$T_{lm}^{E-}(r,\theta,\varphi) \equiv r^{-(l+1)} P_{lm}(\cos\theta)\cos(m\varphi)$$
$$T_{lm}^{O-}(r,\theta,\varphi) \equiv r^{-(l+1)} P_{lm}(\cos\theta)\sin(m\varphi) \quad \text{(A1)}$$

where either the T_{lm}^+ or T_{lm}^- are chosen based upon the boundary conditions of the problem. For a homogeneous field, it is appropriate to use the T_{lm}^+ solutions as shown by (7). The Cartesian derivatives of similar forms for positive powers of r have been derived in (23) and are given by the set of equations (A2) at the bottom of the page. Clearly, these derivatives are representable in terms of spherical harmonics with a common radial factor of r^{n-1} concomitant with a reduced order for the associated Legendre functions. It may be asked if this pattern continues for spatial derivatives of any order. This result may be generalized as follows. Since a component of the field satisfies Laplace's equation, then any spatial derivative of the field also satisfies Laplace's equation. This is represented by the following expansion equations:

$$B(r,\theta,\varphi) = \sum_{lm} A_{lm} T_{lm}^{E\pm}(r,\theta,\varphi) + B_{lm} T_{lm}^{O\pm}(r,\theta,\varphi) \quad \text{(A3)}$$

for the expansion of the field and

$$\frac{dB(r,\theta,\varphi)}{ds} = \sum_{lm} C_{lm} T_{lm}^{E\pm}(r,\theta,\varphi) + D_{lm} T_{lm}^{O\pm}(r,\theta,\varphi)$$

$$\text{(A4)}$$

for the expansion of the derivative of the field where ds represents a differential length and the expansion coefficients are given by $A_{lm}, B_{lm}, C_{lm},$ and D_{lm} (Note that $B_{lm} = D_{lm} = 0$ for $m = 0$). Expanding the spatial derivative gives

$$\frac{dB(r,\theta,\varphi)}{ds} = \frac{\partial r}{\partial s}\frac{\partial B}{\partial r} + \frac{\partial\theta}{\partial s}\frac{\partial B}{\partial\theta} + \frac{\partial\phi}{\partial s}\frac{\partial B}{\partial\phi}. \quad \text{(A5)}$$

The behavior of the various partial components can now be examined with respect to their radial dependence. For the first term, it is noted that $\delta r/\delta s$ does not have units of length and is equal to the cosine of the angle between $\mathbf{dr}$ and $\mathbf{ds}$. On the other hand, $\delta\theta/\delta s$ and $\delta\phi/\delta s$ scale as $1/r$. After performing the $\delta B/\delta r$ operation ($\delta B/\delta\theta$ and $\delta B/\delta\phi$ do not affect the radial dependence), (A5) becomes

$$\frac{dB(r,\theta,\varphi)}{ds}$$
$$= \begin{cases} \sum_{l=1}^{\infty} r^{l-1} \sum_{m=0}^{l} A_{lm} f_{lm}^{E+}(\theta,\varphi) + B_{lm} f_{lm}^{O+}(\theta,\varphi) \\ \sum_{l=0}^{\infty} r^{-(l+2)} \sum_{m=0}^{l} A_{lm} f_{lm}^{E-}(\theta,\varphi) + B_{lm} f_{lm}^{O-}(\theta,\varphi) \end{cases} \quad \text{(A6)}$$

$$T_{nm} \equiv r^n P_{nm}(\cos\theta)\cos(m(\varphi-\psi))$$

$$\frac{\partial T_{nm}}{\partial x} = \frac{r^{n-1}}{2}\left\{ \begin{array}{l} -(1+\delta_{m,0})P_{n-1,m+1}(\cos\theta)\cos((m+1)\varphi - m\psi) \\ +(1-\delta_{m,0})(n+m)(n+m-1)P_{n-1,m-1}(\cos\theta)\cos((m-1)\varphi - m\psi) \end{array} \right\}$$

$$\frac{\partial T_{nm}}{\partial y} = \frac{r^{n-1}}{2}\left\{ \begin{array}{l} -(1+\delta_{m,0})P_{n-1,m+1}(\cos\theta)\sin((m+1)\varphi - m\psi) \\ -(1-\delta_{m,0})(n+m)(n+m-1)P_{n-1,m-1}(\cos\theta)\sin((m-1)\varphi - m\psi) \end{array} \right\}$$

$$\frac{\partial T_{nm}}{\partial z} = r^{n-1}(n+m)P_{n-1,m}(\cos\theta)\cos(m(\varphi-\psi)) \quad \text{(A2)}$$

where f_{LM} is simply a function of angular variables only. Comparison of (A4) to (A6) and equating powers in r gives the following identities:

$$\sum_{m=0}^{l} A_{l+1,m} f_{l+1,m}^{E+}(\theta, \varphi) + B_{l+1,m} f_{l+1,m}^{O+}(\theta, \varphi)$$

$$= \sum_{m=0}^{l} C_{lm} P_{lm}(\cos\theta) \cos(m\varphi) + D_{lm} P_{lm}(\cos\theta) \sin(m\varphi)$$

$$\sum_{m=0}^{l} A_{l-1,m} f_{l-1,m}^{E-}(\theta, \varphi) + B_{l-1,m} f_{l-1,m}^{O-}(\theta, \varphi)$$

$$= \sum_{m=0}^{l} C_{lm} P_{lm}(\cos\theta) \cos(m\varphi) + D_{lm} P_{lm}(\cos\theta) \sin(m\varphi).$$

$$(A7)$$

Clearly the effect of the spatial derivative is to shift the contribution of the A_{lm} and B_{lm} coefficients to a neighboring order. This process is simply repeated for higher derivatives. For the kth spatial derivative, the result is that a particular A_{lm} or B_{lm} coefficient will be found in terms of order $(l \pm k)$.

Since our interest is in homogeneous fields, the following discussion is relevant for only positive powers of r, (T_{lm}^+). From (A7), the only contribution at the origin to the kth spatial derivative of the field arises from the C_0 term, as higher orders vanish at the origin. If this derivative is zero at the origin, then $C_0 = 0$. This in turn requires that all A_{lm} and B_{lm} terms of order $k(l = k)$ to be equal to zero. This implies that there is an equivalence between the nth spatial derivatives to the nth order terms in the spherical harmonic expansion. *If all of the coefficients of nth order in the expansion of the field in terms of spherical harmonics are equal to zero, then all nth order spatial derivatives of the field are identically equal to zero at the origin of the target region.*

REFERENCES

[1] F. A. Jolesz, "Image-guided procedures and the operating room of the future," *Radiology*, vol. 204, pp. 601–612, 1997.

[2] ——, "Interventional and interoperative MRI: A general overview of the field," *J. Magn. Res. Imag.*, vol. 8, pp. 3–6, 1998.

[3] N. G. Cifune, "Open sesame!," *Med. Imag.*, pp. 64–70, Apr. 2000.

[4] E. T. Laskaris and B. Dorri, "Open MRI Superconductive Magnet with Cryogenic-Fluid Cooling," U.S. Patent 5 568 104, Oct. 22, 1996.

[5] B. Dorri, E. T. Laskaris, M. D. Ogle, and T. J. Havens, "Shielded and Open MRI Magnet," U.S. Patent 5 565 831, Oct. 15, 1996.

[6] Y. M. Pulyer, "High Field Strength Magnet Preferably Having Remote Shimming of Field," U.S. Patent 5 049 848, Sept. 17, 1991.

[7] ——, "MRI Device Having High Field Strength Cylindrical Magnet with Two Axially Spaced Electromagnets," U.S. Patent 5 389 879, Feb. 14, 1995.

[8] A. R. Rath, S. B. W. Roeder, and E. Fukushima, "Opposed coil magnet calculation for large sample and unilateral nuclear magnetic resonance," *Rev. Sci. Instrum.*, vol. 56, no. 3, pp. 402–410, Mar. 1985.

[9] I. L. McDougall and J. M. Bird, "Magnet Assembly Having a Plurality of Nested Coaxial Coils," U.S. Patent 4 701 736, Oct. 20, 1987.

[10] I. L. McDougall, P. Hanley, and R. C. Hawkes, "Magnetic Field Generating Assembly," U.S. Patent 5 331 282, July 19, 1994.

[11] B. Dorri and E. T. Laskaris, "Pancake MRI Magnet with Modified Imaging Volume," U.S. Patent 5 428 292, June 27, 1995.

[12] E. T. Laskaris and M. D. Ogle, "Planar Superconducting MRI Magnet," U.S. Patent 5 677 630, Oct. 14, 1997.

[13] Y. M. Pulyer, "Planar Open Magnet for MRI Systems," U.S. Patent 5 477 960, Apr. 28, 1998.

[14] ——, "Planar Open Solenoidal Magnet MRI System," U.S. Patent 5 914 600, June 22, 1999.

[15] ——, "Planar Open Magnet MRI System Having Active Target Field Shimming," U.S. Patent 6 002 255, Dec. 14, 1999.

[16] D. B. Montgomery and R. G. Weggel, *Solenoid Magnet Design*. Malabar, FL: Robert E. Krigger, 1969.

[17] W. Franzen, "Generation of uniform magnetic fields by means of air-core coils," *Rev. Sci. Instrum.*, vol. 33, no. 9, pp. 933–938, Sept. 1962.

[18] J. E. C. Williams, "Superconducting magnets for MRI," *IEEE Trans. Nucl. Sci.*, vol. NS-31, pp. 994–1005, Aug. 1984.

[19] Y. M. Pulyer and S. Patz, "MRI Probe for External Imaging," U.S. Patent 5 572 132, Nov. 5, 1996.

[20] R. K. Cooper and J. A. Jackson, "Remote (inside-out) NMR. I. Remote production of a region of homogeneous magnetic field," *J. Magn. Reson.*, vol. 41, pp. 400–405, 1980.

[21] J. A. Jackson, L. J. Burnett, and J. F. Harmon, "Remote (inside-out) NMR. III. Detection of nuclear magnetic resonance in a remotely produced region of homogeneous magnetic field," *J. Magn. Reson.*, vol. 41, pp. 411–421, 1980.

[22] J. D. Jackson, *Classical Electrodynamics*, 2nd ed. New York: Wiley, 1975, p. 182.

[23] F. Romeo and D. I. Hoult, "Magnet field profiling: Analysis and correcting coil design," *Magn. Reson. Med.*, vol. 1, pp. 44–65, 1984.

[24] M. I. Hrovat, L. Panych, and K. Arvanitis, "Magnetic field mapping to high order, error estimation and analysis of variance," presented at the Soc. Magn. Reson. Med. Conf., Berlin, Germany, 1992.

[25] D. I. Hoult and D. Lee, "Shimming a superconducting nuclear-magnetic-resonance imaging magnet with steel," *Rev. Sci. Instrum.*, vol. 56, pp. 131–135, Jan. 1985.